Aerosol and Air Quality Research, x: 1–13, xxxx

ISSN: 1680-8584 print / 2071-1409 online
doi: 10.4209/aaqr.2016.05.0195

Evaluating the Effects of Springtime Dust Storms over Beijing and the Associated Characteristics of Sub-Micron Aerosol

Peng Xu[1,2], Junke Zhang[2†], Dongsheng Ji[2], Zirui Liu[2], Guiqian Tang[2], Bo Hu[2], Changsheng Jiang[1*], Yuesi Wang[2]**

[1] Key Laboratory of Eco-environments in Three Gorges Reservoir Region, Ministry of Education, Chongqing Key Laboratory of Agricultural Resources and Environment, College of Resources and Environment, Department of Environmental Science and Engineering, Southwest University, Chongqing 400716, China
[2] State Key Laboratory of Atmospheric Boundary Layer Physics and Atmospheric Chemistry (LAPC), Institute of Atmospheric Physics, Chinese Academy of Sciences, Beijing 100029, China

ABSTRACT

In order to understand the characteristics, sources and processes of non-refractory submicron particles (NR-PM_1), an Aerodyne high-resolution time-of-flight aerosol mass spectrometer (HR-ToF-AMS) was deployed to acquire observational data during the spring (April 1 to 30) in Beijing, China, in 2012. Based on PM_{10}, $PM_{2.5}$ and NR-PM_1 mass concentrations observation, satellite images and the back trajectory analysis, one haze and dust storm episodes were recorded during the campaign, in addition, one clean episodes was also added to the comparison as a reference. The NR-PM_1 mass concentration was 97 μg m^{-3} during the haze episodes, while it was approximately 12 times and 1.7 times that on the clean and dust episodes, respectively. In addition, the secondary inorganic aerosol (sulfate, nitrate and ammonium) contributed the largest fraction of NR-PM_1 (69%) during the haze episodes. The dust storms originated from the northwestern caused the PM_{10} peaking at 826 μg m^{-3}, with an average of 364 ± 186 μg m^{-3} and higher than the haze episodes (241 μg m^{-3}). In addition, compared to the clean episodes (the NR-PM_1 mass was 8 μg m^{-3}), the dust storms caused the average NR-PM_1 mass reaching 56 μg m^{-3}, corresponding to the secondary components significantly increased, including sulfate (9.5 μg m^{-3}), nitrate (8 μg m^{-3}), ammonium (6 μg m^{-3}) and OOA (6 μg m^{-3}). The backward trajectory clustering analysis indicated the air mass from the southeast (at a frequency more than 30%) contained the higher NR-PM_1 concentration (more than 80 μg m^{-3}) corresponding to the higher sulfate, nitrate and ammonium contributions.

Keywords: NR-PM_1; Organic aerosols; Dust storm; Springtime; Beijing.

INTRODUCTION

Fine particles ($PM_{2.5}$ and PM_1, defined as particulate matter with an aerodynamic diameter of less than 2.5 μm and 1 μm, respectively) have significantly impacted climate change and visibility and also threaten human health (Guo *et al.*, 2014). As the political, economic and cultural center of China, Beijing frequently encountered severe haze pollution as a result of the high concentrations of fine particles (Sun *et al.*, 2013b; Guo *et al.*, 2014). Because fine particles are a complicated mixture of various species, a deep understanding of the variations in the chemical properties of fine particles is essential for source identification and pollution control (Huang *et al.*, 2011).

Vehicle emissions, cooking and the secondary formation of aerosols from anthropogenic precursors have all been identified as important sources of fine particulate in the Beijing area (Huang *et al.*, 2010; Sun *et al.*, 2010; Sun *et al.*, 2013b; Zhang *et al.*, 2014; Hu *et al.*, 2016). Dust storms are also an important source of fine particles and can cause adverse health effects for humans (Wang *et al.*, 2013). Therefore, it is very important and meaningful to study the chemical composition and the processes associated with dust particles. The Gobi Desert, located in south Mongolia and north China, is one of the major source regions of dust storms (Arimoto *et al.*, 2006). In spring, the surface dust of the Gobi Desert can internally mix with secondary compounds through coagulation and heterogeneous reactions while dust

† Now at Faculty of Geosciences and Environmental Engineering, Southwest Jiaotong University, Chengdu 611756, China.

* Corresponding author.
E-mail address: Jiangcs@126.com
** Corresponding author.
Tel.: +86 01082080530; Fax: +86 01062362389
E-mail address: wys@mail.iap.ac.cn

particles are transported (Tobo *et al.*, 2010; Zamora *et al.*, 2011; Wang *et al.*, 2012a).

Most of the previous studies about particles rely on filter sampling followed by laboratory analysis, a method that has some drawbacks, such as the long amount of time necessary to collect particulate matter, laboriousness, low resolution (Huang *et al.*, 2011) and poor capacity for deep analysis of organic aerosols (Hildebrandt *et al.*, 2010). In recent years, high-resolution time-of-flight aerosol mass spectrometers were widely used to characterize the main species of submicron aerosols (Canagaratna *et al.*, 2007; Jimenez *et al.*, 2009; Huang *et al.*, 2010). In particular, based on the high resolution characteristics of the HR-ToF-AMS, multiple organic aerosol (OA) sources have be identified and recognized by combining the positive matrix factorization (PMF) model with the high-resolution OA mass spectral matrix (Ulbrich*et al.*, 2009). Although many studies have been conducted in Beijing to evaluate the composition of submicron particles using HR-ToF-AMS, these observations have mainly been carried out in the summer, autumn and winter (Huang *et al.*, 2010; Sun *et al.*, 2013b; Zhang *et al.*, 2014; Chen *et al.*, 2015; Xu *et al.*, 2015; Zhang *et al.*, 2016). Although Sun *et al.* (2015) used Aerosol Chemical Speciation Monitors (ACSM) to analyze the variation of submicron particles in spring, the elemental composition and source apportionment of the organic aerosol were not studied. More studies are needed, especially to analyze the characteristics, the elemental compositions and source apportionment of submicron particles in the springtime. In addition, the frequent dust storms occurring in spring could impact the submicron particles.

The objective of this work is to contribute to the chemical characterization, elemental composition and source apportionment of submicron particles and to characterize the relative humidity effects on submicron particles. This work also aims to investigate how dust storm episodes could influence the chemical composition of submicron particles in an urban site, such as Beijing.

EXPERIMENTAL METHODS

Sampling Site and Sampling Period

This study was carried out in the courtyard of the Institute of Atmospheric Physics (IAP, 39.97°N, 116.37°E) during April 2012. The site was located between the north 3rd and 4th ring road in Beijing. It is approximately 1 km from the 3rd ring road, 200 m west of the G6 Highway (which runs north-south) and 50 m south of Beitucheng West Road (which runs east-west). The HR-ToF-AMS instrument was installed inside the two story laboratory building, and the ambient air sampling port was installed approximately 12 m above the ground. This site was surrounded by heavy traffic, restaurants, residential areas, and research institutions, and the local environment is typical of urban pollution in Beijing (Liu *et al.*, 2016)

Instrumentation and Sampling

An Aerodyne high-resolution time-of-flight aerosol mass spectrometer (HR-ToF-AMS) was introduced by DeCarlo *et al.* (2006). The HR-ToF-AMS was operated in the sensitive V-mode and the high mass resolution W-mode, alternating every 5 min. In V-mode, the aerosol mass spectrometer (AMS) cycled through mass spectrum (MS) mode and particle time-of-flight (PToF) mode every 30 s. No PToF data were sampled in W-mode because of the low signal-to-noise (S/N) ratio. The HR-ToF-AMS was calibrated for inlet flow, ionization efficiency (IE) and particle sizing at the beginning and end of the study following the standard protocols (Jayne *et al.*, 2000; Jimenez *et al.*, 2003). The detection limit (DL) of the HR-ToF-AMS is related to the resolution of the instrument, the signal-to-noise ratio, the vaporization temperature and the ionizer background (DeCarlo *et al.*, 2006). The ionizer background, with influence on the DL, includes measurements of elevated aerosol mass concentrations, short-term instrument history and long-term instrument contamination (Drewnick *et al.*, 2009). In this study, the DL of each individual species is taken as three times the standard deviation of the corresponding signal of particle-free air (DeCarlo *et al.*, 2006; Sun *et al.*, 2009). The 5-min DL of organics, nitrate, sulfate, ammonium and chloride were determined to be 0.056, 0.006, 0.008, 0.04 and 0.014 μg m^{-3}, respectively. In addition to the HR-ToF-AMS, a Thermo TEOM1405 (Filter Dynamic Measurement System) was used to measure the mass concentrations of PM_{10} and $PM_{2.5}$. Meteorological data, such as temperature (T), relative humidity (RH) and wind speed/direction (WS/WD), were also available from an automatic meteorological observation instrument (Milos520, Vaisala, Finland).

Data Analysis

The standard ToF-AMS data analysis software packages SQUIRREL version 1.50 and PIKA version 1.09, downloaded from the ToF-AMS-Resources webpage (http://cires.colorado.edu/jimenez-group/ToFAMSResources), were used to generate unit and high-resolution mass spectra from the V-mode and W-mode data, respectively (He *et al.*, 2011; Zhang *et al.*, 2014). A previous study proposed that the collection efficiency (CE) is affected by high aerosol acidity, high relative humidity and a high ammonium nitrate mass fraction (ANMF > 0.4) (Middlebrook *et al.*, 2012). In this study, a silica-gel desiccant was used to keep the relative humidity below 40% in the sampling line, and the aerosol acidity was nearly neutral. The ANMF was at times higher than 0.4. Therefore, a variable CE, based on the higher ANMF value, was applied, CE_{dry} = max (0.45, 0.0833 + 0.9167 × ANMF). The default relative ionization efficiency (RIE) values, 1.1, 1.3 and 1.4, were applied to calculate the mass concentration of nitrate, chloride and the organic components, respectively. RIE values of 3.9 and 1.0 were used to calculate ammonium and sulfate, respectively. These two values were determined from IE calibrations using ammonium nitrate and ammonium sulfate particles. The elemental analysis of the organic components identified by positive matrix factorization (PMF) was carried out using previously described methods (Aiken *et al.*, 2007, 2008).

Positive matrix factorization (PMF) was used to analyze the high-resolution mass spectra (HRMS) (m/z 10-120) obtained using HR-ToF-AMS to identify the major organic

components (Reff *et al.*, 2007). The HRMS data and error matrices were generated as outlined in DeCarlo *et al.* (2010). Data and error matrices used as inputs for the PMF analysis were generated with the default fragmentation waves in PIKA. The noise values were calculated as the sum of the electronic and Poisson ion-counting errors for the relevant high-resolution ion fragment (Allan *et al.*, 2003; Ulbrich *et al.*, 2009). Ions with a S/N ratio < 0.2 were removed from the HRMS data and error matrices before the PMF analysis. Weak ions (0.2 < SNR < 2) were downweighted by a factor of 3, and bad ions (SNR < 0.2) were removed from the analysis (Paatero and Hopke, 2003). Solutions for one to eight factors were explored with varying rotational parameters ($-1 \leq$ FPEAK ≤ 1, in increments of 0.1). Finally, the 3-factor was chosen as the optimal solution for this analysis.

RESULTS AND DISCUSSION

Aerosol Components by Positive Matrix Factorization

In this sampling campaign, positive matrix factorization analysis of the high resolution mass spectrometer (HRMS) data identified three organic aerosol components: oxygenated organic aerosol (OOA), cooking organic aerosol (COA) and hydrocarbon organic aerosol (HOA) (Fig. 1). Previous studies noted that OOA formed from secondary organic aerosol through a gas-to-particle conversion (Huang *et al.*, 2011, 2012; Zhang *et al.*, 2014). The O/C ratio of the OOA identified in this study was 0.79 (Fig. 1(a)), higher than the O/C ratios of OOA reported in other districts, including winter in Beijing (0.62) (Zhang *et al.*, 2014), summer in Beijing (0.47) (Huang *et al.*, 2010), and autumn in Kaiping (0.52) (He *et al.*, 2011). The high-resolution mass spectra of OOA were characterized by prominent $C_xH_yO_z$ fragments, especially CO_2^+ (m/z 44) and CO^+ (m/z 28). The time series trend of OOA typically correlated well with tracer indicators ($NO_3 + SO_4$) (Fig. 1(a1)), and the OOA had the best correlations with sulfate ($R^2 = 0.76$) and nitrate ($R^2 = 0.58$), consistent with the results from a study conducted in Fresno, CA (Ge *et al.*, 2012).

Cooking activity (including fuel and food materials in cooking) accounts for a significant fraction of the organic aerosol at all urban sites (Chow *et al.*, 2007; Huang *et al.*, 2010; Sun *et al.*, 2010; Zhang *et al.*, 2014). The mass spectra of the COA were characterized by the prominent ion series of $C_xH_y^+$, especially $C_nH_{2n}^+$, including m/z 41 and m/z 55 (Zhang *et al.*, 2014; Hu *et al.*, 2016; Zhang *et al.*, 2016). This result indicates a significant presence of unsaturated organic compounds (e.g., unsaturated fatty acids) and is consistent with the MS characteristics of primary emissions from Chinese cooking (He *et al.*, 2010). The COA showed correlations with a few $C_6H_{10}O$ ions ($R^2 = 0.48$) (Fig. 1(b1)). These ions were tracer indicators of the spectral sources of cooking emissions and could be used as spectral markers for COA (Zhang *et al.*, 2014).

Previous studies reported that HOA can typically be attributed to fossil fuel combustion (Lanz *et al.*, 2007; Zhang *et al.*, 2007; Ulbrich *et al.*, 2009). Gasoline and diesel fuel combustion emissions consist mainly of n-alkanes, branched alkanes, cycloalkanes and aromatics (Canagaratna *et al.*, 2004), leading to a high signal for ion series $C_nH_{2n}^+$ and $C_nH_{2n-1}^+$ in the HRMS. Higher m/z (57) and lower O/C ratios (< 0.2) are typically used to identify HOA; nearly all exhaust aerosols from diesel trucks and gasoline vehicles have their most prominent peaks at m/z 57 (Mohr *et al.*, 2009). In this study, the HOA was characterized by prominent hydrocarbon ion peaks at m/z 41, 43, 55, and 57 (Fig. 1(c)). The O/C ratio (0.14) was dramatically higher than the value of 0.03, which was measured during the characterization of emissions from a motor vehicle (Mohr *et al.*, 2009). Sun *et al.* (2011b) deployed an AMS on two high-traffic highways in New York City and found the O/C ratios were only 0.04. However, the O/C ratios measured in Beijing (0.17) (Huang *et al.*, 2010) and Shanghai (0.16) (Huang *et al.*, 2012) were similar to the result of this study. The HOA and NO_x were

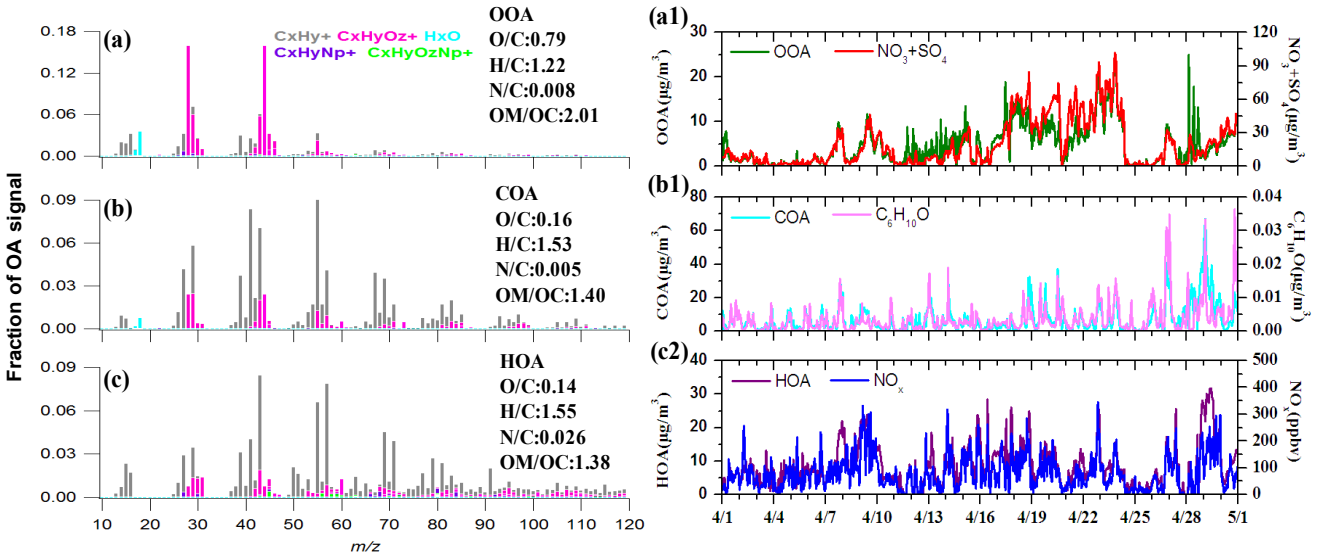

Fig. 1. The HRMS profiles of the (a) OOA, (b) COA and (c) HOA identified by PMF and the time series of (a1) the OOA and $NO_3 + SO_4$; (b1) the COA and $C_6H_{10}O$; (c1) the HOA and NO_x.

well correlated (R^2 = 0.60) and had pronounced peaks during the morning and night, corresponding to traffic emissions (Fig. 1(c1)). These facts indicate that HOA is likely a surrogate for the combustion of primary organic aerosol (POA), a conclusion reached in many other studies (Aiken *et al.*, 2009; Ulbrich *et al.*, 2009).

Characteristics of NR-PM$_1$

Mass Concentrations, Composition and Size Distribution of NR-PM$_1$

Total non-refractory submicron particle (NR-PM$_1$) mass concentration ranged from 0.3 to 209.5 μg m^{-3}, with an average of 49.7 ± 40.2 μg m^{-3} (Fig. 2(d)). This mean value was lower than previously reported values of NR-PM$_1$ mass concentrations measured using an AMS in the Beijing district. For example, the mean mass concentrations during the summers of 2006 and 2008 were 80.0 μg m^{-3} (Sun *et al.*, 2010) and 63.1 μg m^{-3} (Huang *et al.*, 2010), respectively; the mean mass concentrations during the winters of 2011 and 2012 were 66.8 μg m^{-3} (Sun *et al.*, 2013b) and 89.3 μg m^{-3} (Zhang *et al.*, 2014), respectively. However, values in this study approached the mean mass concentrations found during the spring of 2012 in Beijing (52 μg m^{-3}) (Sun *et al.*, 2015). Compared with other countries, this result is much higher than other urban districts, such as New York City (11.0 μg m^{-3}) (Sun *et al.*, 2011a) and Pittsburgh (14.8 μg m^{-3}) (Zhang *et al.*, 2005); NR-PM$_1$ mass concentrations were 10–30 μg m^{-3} in Europe (Kubelova *et al.*, 2015). In some atmospheric background areas in China, the NR-PM$_1$ mass concentrations were much lower than in the urban areas; for example, Du *et al.* (2015) measured mass concentration of 11.9 μg m^{-3} which at a national background monitoring station in the Tibetan plateau.

As mentioned in Section 3.1, OA components (OOA, COA, HOA) were identified using the PMF model. The OOA concentration varied within the range of 0.01–24.99 μg m^{-3}, with an average value of 4.65 μg m^{-3}, and accounted for 23% (Fig. 3(b)) of the OA. The HOA varied between 0.01 μg m^{-3} and 31.7 μg m^{-3}, with an average of 8.5 μg m^{-3}, and contributed 42% (Fig. 3(b)) to the OA, which indicates this research district was influenced by the fossil fuel combustion during the observation period. The COA varied within the range of 0.02–66.9 μg m^{-3}, with a mean value of 7.2 μg m^{-3}, and accounted for 35% (Fig. 3(b)) of the OA. This result was higher than most reported values; for example, the COA accounted for 20% of the organic aerosol observed in the winter in Beijing (Zhang *et al.*, 2014) and 24.4% of the organic aerosol observed in the summer (Huang *et al.*, 2010). The COA accounts for 16% of organic aerosol in New York City (Sun *et al.*, 2011a) and 17% of organic aerosol in Barcelona (Mohr *et al.*, 2012).

The average chemical composition of NR-PM$_1$ was showed in Fig. 3(a). The organics accounted for 51% of the NR-PM$_1$ components, followed by sulfate (18%), nitrate (16%), ammonium (12%) and chloride (3%). Compared with previous studies on the average contribution of organics, the organics contribution value (51%) measured in the present study was higher than those observed during the

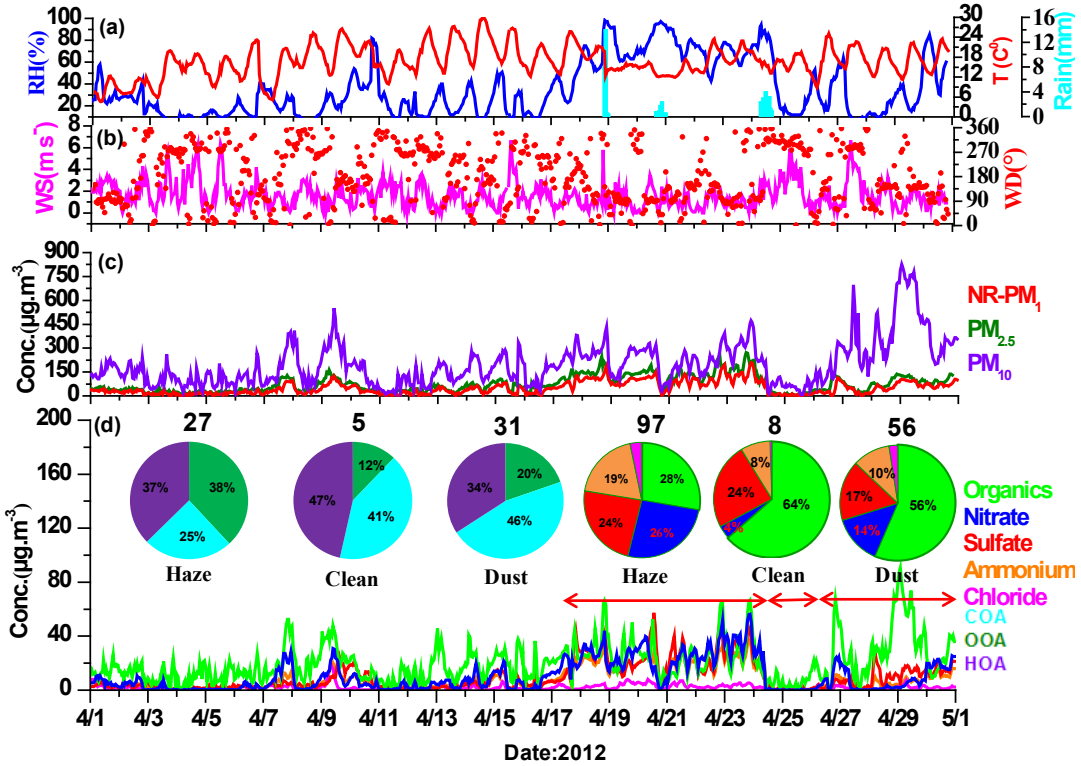

Fig. 2. Temporal evolution of (a) ambient temperature, relative humidity and rainfall; (b) wind direction and wind speed; (c) NR-PM$_1$, PM$_{2.5}$ and PM$_{10}$ mass concentrations; (d) NR-PM$_1$ species concentrations and the pie charts in (d) showed the average chemical composition during the haze, clean and dust episodes.

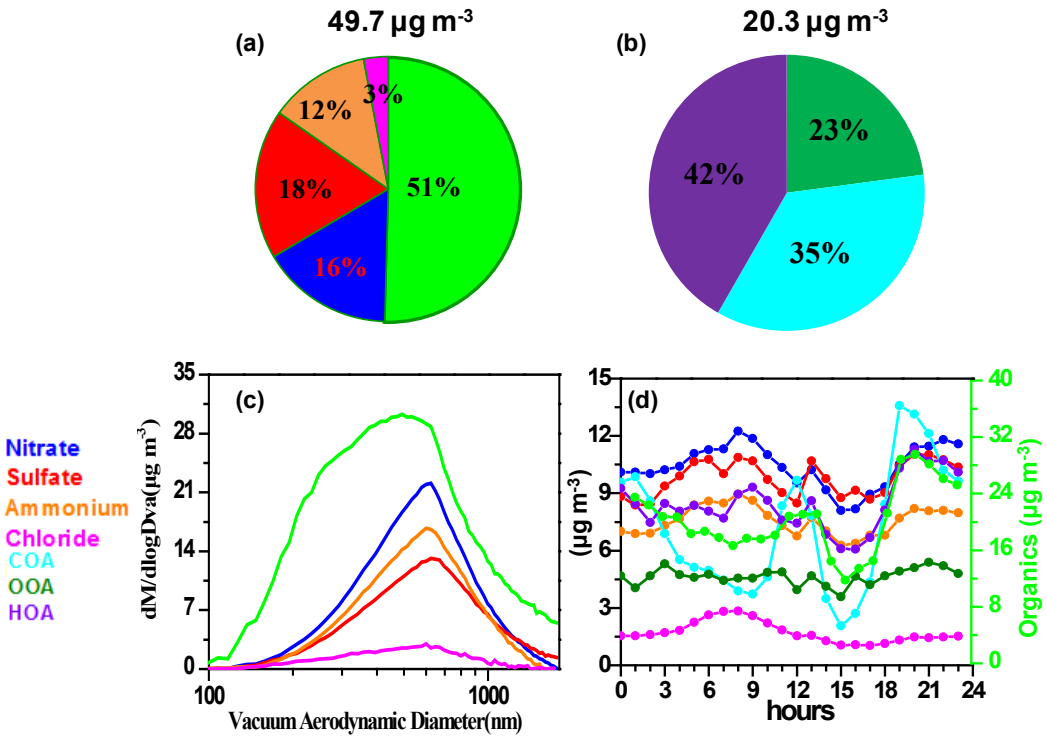

Fig. 3. The mean NR-PM_1 (a) and OA compositions (b); (c) the average mass size distributions of NR-PM_1 species; (d) the average diurnal variation of NR-PM_1 species.

summer in Beijing in 2006 (35%) (Sun *et al.*, 2010) and 2008 (39%) (Huang *et al.*, 2010) but approximated those measured during the winter in Beijing in 2011 (52%) (Sun *et al.*, 2013b) and 2012 (50%) (Zhang *et al.*, 2014).

Organic aerosol showed a broader distribution and appeared in accumulation mode, peaking around 500–550 nm in vacuum aerodynamic diameter (D_{va}), whereas inorganic species (sulfate, nitrate and ammonium) peaked at 600 nm (Fig. 3(c)). The organics also had a smaller ultrafine mode (peaking < 150 nm), this mode was dominated by HOA, which generally is non-hygroscopic with low scavenging rates (Sun *et al.*, 2011a).

The Diurnal Variation of NR-PM_1

The diurnal variation in organics was characterized by two pronounced peaks at noon (12:00–13:00; 21 μg m^{-3}) and at night (19:00–20:00; 29 μg m^{-3}) (Fig. 3(d)). The noon peaked is related to cooking emission; the evening peak is derived from a combination of cooking and traffic emissions (Huang *et al.*, 2010; Zhang *et al.*, 2014; Sun *et al.*, 2015). The OOA showed a mostly stable diurnal signal, and the highest and lowest values occurred at night (5.37 μg m^{-3}) and at noon (3.57 μg m^{-3}) (Fig. 3(d)), respectively. The COA showed pronounced diurnal variation with peaks corresponding to meal times appearing at noon (12:00) and in the evening (20:00), having values of 13.1 μg m^{-3} and 9.7 μg m^{-3}, respectively (Fig. 3(d)). This phenomenon indicated that the local cooking-related emission sources play a very important role. The HOA showed a clear diurnal variation pattern. The highest and lowest values occurred in the afternoon (16:00) and at night (20:00), with values of 6.0 μg m^{-3} and 11.3 μg m^{-3}, respectively. The HOA always increased between 16:00 and 20:00, similar to the COA (Fig. 3(d)).

Sulfate showed significant diurnal variation and appeared as three small peaks throughout the day. The sulfate concentrations during the peak periods were 10.8, 10.6 and 11.0 μg m^{-3}, corresponding to the morning (8:00), noon (13:00) and the evening (20:00), respectively (Fig. 3(d)). The morning and evening sulfate peaks depended on the dilution effect of the planetary boundary layer and traffic emission; the noon sulfate peak was related to daytime photochemical sulfate production (Sun *et al.*, 2015). Nitrate concentrations continuously increased throughout the morning, peaking at 8:00 (12.2 μg m^{-3}). Nitrate was also characterized by a pronounced evening peak (20:00–21:00), corresponding to 11.4 μg m^{-3} (Fig. 3(d)). The diurnal variation in ammonium was similar to sulfate. Ammonium appeared as two small peaks: one in the morning (8:00) and one in the evening (20:00), where the corresponding concentrations were 8.9 μg m^{-3} and 8.2 μg m^{-3}, respectively (Fig. 3(d)). The diurnal variations of sulfate and ammonium were different from others studies. For example, Huang *et al.* (2010) found the diurnal variation of sulfate and ammonium to be a relatively flat trend, except for a small increased in the afternoon during summer. Zhang *et al.* (2014) found that the sulfate, nitrate and ammonium mass concentrations obviously decreased in the morning during winter. These seasonal differences likely impact the gas-to-particle partitioning and aqueous-phase processing, and the planetary boundary layer plays a significant role in spring. The chloride concentration appeared peak in the morning

(Fig. 3(d)); this phenomenon was similar to a study conducted in the spring by Sun *et al.* (2015) and a study conducted in the summer by Huang *et al.* (2010) but was different from a study conducted in winter by Zhang *et al.* (2014).

Relative Humidity (RH) Effects on chemical Components

The mass concentrations of the NR-PM_1 species appeared to increase as function of relative humidity and reached their highest values at the 60%–70% RH level. When the RH was more than 70%, the mass concentration decreased slightly (Fig. 4(a)). The OA components (OOA, COA and HOA) showed a different dependence on RH (Fig. 4(b)). The mass concentrations, chemical compositions and rate of increase appeared at different RH levels. At low RH (< 50%), the average NR-PM_1 and OA mass concentrations were 34.4 μg m^{-3} and 18.5 μg m^{-3}, respectively. Organics dominated the NR-PM_1 composition, accounting for 58% of NR-PM_1, and showed the largest mass concentration rate increase (8.5 μg m^{-3}/10% RH) among all the NR-PM_1 components. POA (COA+ HOA) dominated the OA composition at low RH, accounting for 81% of OA (Fig. 4(c)). At high RH (> 50%), the average NR-PM_1 and OA mass concentrations were 88.1 μg m^{-3} and 24.6 μg m^{-3}, respectively, and the secondary inorganic species (nitrate + sulfate + ammonium) dominated the NR-PM_1 composition, accounting for 67% of NR-PM_1, which of nitrate represented 25%, sulfate represented 24%, and ammonium represented 18% (Fig. 4(d)). Nitrate showed the largest mass concentration rate increase (9.8 μg m^{-3}/RH 10%), followed by sulfate (6.5 μg m^{-3}/10% RH), and ammonium (6.5 μg m^{-3}/10% RH), indicating the significant effect of RH on secondary inorganic species. The secondary inorganic species (nitrate, sulfate and ammonium) appeared to rapidly increase because the atmospheric environment exists at a high RH, and the aqueous-phase oxidation is much faster than gas-phase oxidation processes (Seinfeld and Pandis, 2006). The oxidation state in the aqueous-phase relies on droplet pH and mass concentrations of oxidants (Shen *et al.*, 2012). Similar to NR-PM_1 species, the OA components presented synchronous enhancements at high RH levels, especially the OOA, which accounted for 36% of OA and showed the largest enhancement (from 3.5 μg m^{-3} increased to 8.9 μg m^{-3}). RH showed a weaker effect on COA and HOA likely due to their lower degree of oxidation and hygroscopicity (Sun *et al.*, 2013a).

The Effects of Dust on Submicron Aerosol

The weather forecast was gathered from the National Satellite meteorological center and combined with mass concentrations of $PM_{2.5}$ and PM_{10}. This portion of the study was divided into three episodes: (i) Haze episodes (April 17–24); (ii) Clean episodes (April 25th); (iii) Dust episodes (April 26–30) (Fig. 2(d)).

Meteorological conditions were predominant factors during the clean period. As shown in Figs. 1(a) and 1(b), wind speed was consistently enhanced, with an average of 2.7 m s^{-1}, which prevailed from the northwest, while RH continuously decreased and reached low levels (with an average of 33.7%), and temperature varied only slightly. Such meteorological conditions would rapidly obliterate local pollutants, leading to the average NR-PM_1, $PM_{2.5}$ and PM_{10} mass concentrations being 8, 11 and 54 μg m^{-3}, respectively, during the clean episodes (Fig. 1(c)). The organics, nitrate, sulfate and ammonium accounted for 64%, 4%, 24% and 8% of NR-PM_1, respectively (Fig. 1(d)).

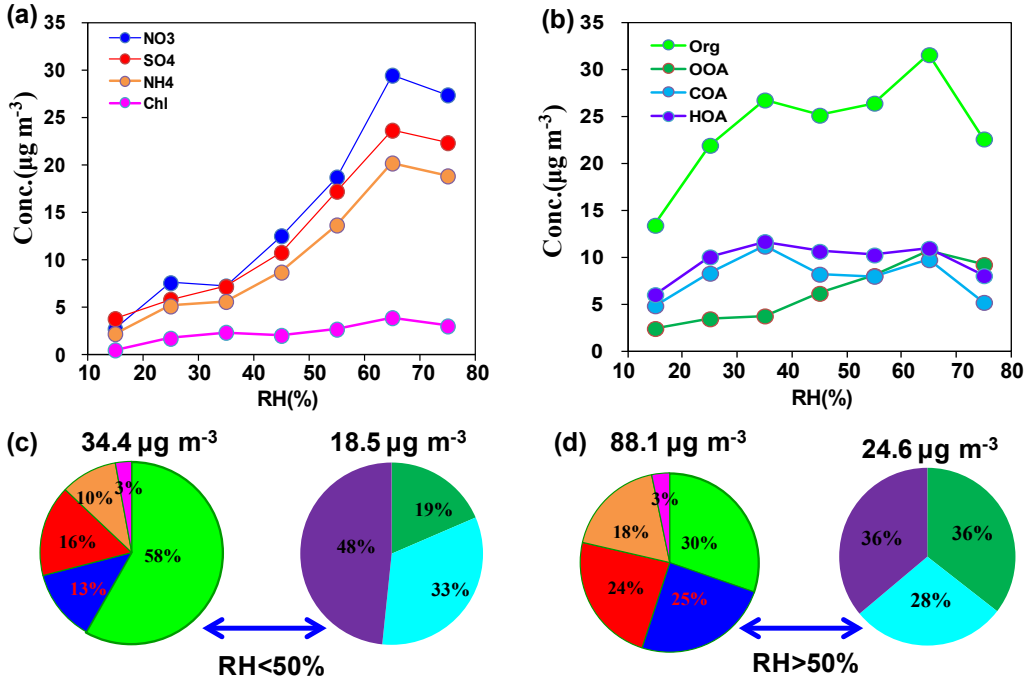

Fig. 4. The variation of mass concentrations of NR-PM_1 species (a) and OA components (b) as a function of relative humidity; (c) the average chemical compositions of NR-PM_1 and OA at low relative humidity (RH < 50%) and high relative humidity (RH > 50%) levels.

The average NR-PM_1, $PM_{2.5}$ and PM_{10} mass concentrations were 97, 127 and 241 μg m^{-3}, respectively, during the haze episodes (Fig. 1(c)). The highest average NR-PM_1 chemical species mass concentration was for the organics (26.8 μg m^{-3}), followed by nitrate (25.6 μg m^{-3}), sulfate (23.2 μg m^{-3}), ammonium (18.7 μg m^{-3}), and chloride (3.2 μg m^{-3}). In addition, the chemical species composition of NR-PM_1 contained organics, sulfate, nitrate, ammonium and chloride at 28%, 24%, 26%, 19% and 3%, respectively (Fig. 1(d)). Secondary inorganic aerosol (sulfate, nitrate and ammonium) contributed the largest fraction of NR-PM_1 during the haze episodes (66%). Sun *et al.* (2015) indicated that photochemical production, especially higher O_3 and strong solar radiation, plays a dominant role in affecting secondary aerosol formation. In addition, the precursors of NO_x and SO_2 also affect secondary aerosol formation. Pan *et al.* (2016) put forward the nitrogen center theory, indicating that controlling NO_x emissions should be a priority to decrease secondary inorganic aerosol formation in haze pollution. However, heterogeneous formation mechanisms of chemical production that occur primarily in the droplet mode have also been shown to be important contributors of secondary aerosol during fine particles pollution events (Wang *et al.*, 2012b; Sun *et al.*, 2013c). Levy *et al.* (2014) also indicated that the fine particles could undergo rapid hygroscopic growth, and these particles are then characterized by high surface area and low density, which can be easy impacted by the heterogeneous formation mechanisms, leading to more accumulation of secondary aerosol. Therefore, nitrate, sulfate and ammonium were the major contributor to NR-PM_1 during haze pollution.

The amount of rainfall for the three recorded rainfall events ranged from 0.2 mm to 13.8 mm during the haze episodes. The hourly values, which were higher than 5 mm, appeared at 20:00 (7.8 mm) and 21:00 (13.8 mm) on the April 18. Although the amount of rainfall was small, NR-PM_1 and its chemical components significantly decreased. Huo *et al.* (2010) showed that with increasing rainfall, the dilution of particulate matter is gradually enhanced. Scavenging of particles through falling precipitation is a major removal mechanism, especially in particles sizes between 0.1 and 10 μm. Rainfall between 1 and 5 mm is most important for washout (Quérel *et al.*, 2013). We *et al.* (2015) also studied how rainfall can reduce the fine particle mass concentrations in the atmosphere and found that washing significantly affected the air quality.

Large-scale dust storms with high PM_{10} levels occurred twice in the Middle East region of Inner Mongolia on the April 26th and 27th, and dust was still heavy in the atmosphere on April 28th during the dust episodes (dust episodes spanned April 26–30). The 72 h backward trajectory indicated that the dust storm air mass arrived over the observation site from the northwest region (Fig. 5). The weather at the observation site was relatively warm (T: 17.4 ± 3.8°C) and dry (RH: 31% ± 21%). The wind speed ranged from 0.1 to 6.7 m s^{-1}, with an average of 1.5 ± 1.2 m s^{-1}, and the wind was predominantly from the northwest during the dust episodes (Figs. 1(a) and 1(b)). The dust weather caused the PM_{10} mass concentration reaching 826 μg m^{-3}, with an average value of 364 ± 186 μg m^{-3}. Additionally, the NR-PM_1 and $PM_{2.5}$ mass concentrations also increased, and the average mass concentrations were 56 ± 28 μg m^{-3} and 72 ± 36 μg m^{-3}, respectively (Fig. 1(c)). Wang *et al.* (2014) indicated that the surface soil in the Gobi Desert and the Loess Plateau contained some fine particles. Previous research on the impacts of dust storms on the chemical species mass concentrations of aerosol found that, in the presence of dust storms, most of the airborne particulate originated

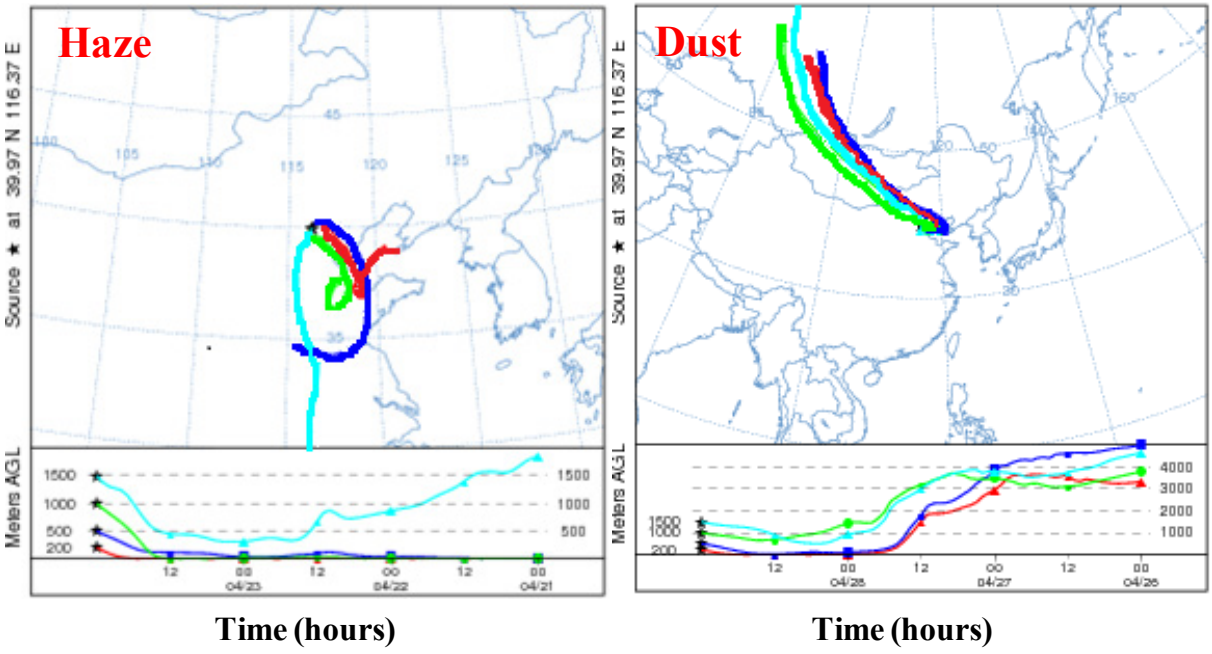

Fig. 5. Backward trajectories of air masses reaching Beijing during the haze episodes (Haze episodes from 17 April to 24 April) and dust episodes (Dust episodes from 26 April to 30 April).

from Gobi Desert soil (Wang *et al.*, 2011, 2013). Compared to the clean episodes (organics, nitrate, sulfate and ammonium mass concentrations of NR-PM_1 were 4.5, 0.2, 1.7, 0.5 μg m^{-3}, respectively), the organics, sulfate, nitrate and ammonium mass concentrations reached to 30.7, 8.0, 9.5, 6.0 μg m^{-3}, respectively. The organics increased rapidly and accounted for 56% of NR-PM_1 species. This indicates dust aerosol could contribute a large portion of the organics. When dust processes experience high ambient temperatures and low relative humidity, enhanced photochemical oxidation may lead to more production of OOA (6.1 μg m^{-3}), the OOA accounted for 20% of OA, and compared to clean period, OOA increased 5.5 μg m^{-3}.

Nitrate and sulfate mass concentrations were enhanced during dust episodes but were still much lower than during the haze episodes. This phenomenon can be explained by the formation mechanism and emission sources of sulfate and nitrate during dust process (Wang *et al.*, 2014). Heterogeneous conversion of nitrate and sulfate on dust particles is sensitive to humidity, and their formation efficiency decreases with decreases in humidity (Zhang *et al.*, 1999). Because the humidity was low in the dust episodes (average of 31% ± 21%), it would have been difficult to form nitrate and sulfate through heterogeneous reactions on the dust particles. The dust particles can absorb sulfuric acid and nitric acid (gas and droplets) formed through heterogeneous reaction of SO_2, NO_x, OH, O_2, H_2O_2 (Wang *et al.*, 2016), leading to the formation of nitrate and sulfate during the dust process. As shown by the backward trajectories (Fig. 5), the heavily polluted and clean air mass originated south and northwest during the haze and dust periods, respectively. Because of the low concentrations of NO_x and SO_2 precursors during the dust process, homogeneous formation of sulfate and nitrate is likely not efficient. During the dust episodes, the average daily mass concentrations of nitrate and sulfate were 7.1, 6.1, 19.2 μg m^{-3} and 3.2, 4.2, 15.3 μg m^{-3} on April 26, 27, 30, respectively; the nitrate mass concentrations were higher than the sulfate concentrations. This phenomenon may be explained as follows: the main formation pathways of nitrate and sulfate during the dust process are photo-oxidation of NO_2 and SO_2 via the OH radical, but the nitrate formation is approximately 10 times faster than the sulfate formation (Wang *et al.*, 2013), yielding higher nitrate concentrations. Furthermore, nitrate, sulfate and ammonium can also be produced in submicron particles as $(NH_4)_2SO_4$, NH_4HSO_4, NH_4NO_3 during the dust process (Wang *et al.*, 2014).

Elemental Composition of the Organic Aerosol

The high-resolution organic mass spectra were used to determine the elemental composition of C, H, O, N and the mass ratios of the OM/OC (the ratio of organic mass/organic carbon mass) of the OA. The H/C and N/C ratios varied within a range of 1.37–1.81 and 0.003–0.026, with mean values of 1.59 ± 0.1 and 0.01 ± 0.005, respectively (Fig. 6(a)); the time series of the O/C and OM/OC ratios varied consistently in the ranges of 0.11–0.57 and 1.21–1.93, with mean values of 0.33 ± 0.09 and 1.55 ± 0.15, respectively (Fig. 6(a)). The average values of H/C (1.62), N/C (0.02), O/C (0.41) and OM/OC (1.71) that Aiken *et al.* (2008) found at the ground site in Mexico City were slightly higher than the results of the present study (H/C:1.59, N/C:0.01, O/C:0.33 and OM/OC:1.55). However, the results of the present study were close to those observed using AMS at an urban site in New York City (1.49, 0.01, 0.36 and 1.62) by Sun *et al.* (2011b) and in Beijing (1.44, 0.01, 0.34 and 1.62) by Zhang *et al.* (2014). The elemental ratios are affected by the elemental analysis method calibration, the correction for interferences in ambient air and the improved fragmentation table for ambient organic aerosol (Aiken *et al.*, 2008). The O/C ratio is regarded as a good reference for the oxidation state and photochemical age of the OA (Jimenez *et al.*, 2009; Ng *et al.*, 2010). Hu *et al.* (2016) indicated that the regression slopes between OOA and Ox (O_3+NO_2) in photochemically processed urban emissions provide a metric to investigate the relative efficiency of secondary organic aerosol formation versus O_3 formation during photochemical oxidation. The atmospheric oxidation state and photochemical oxidation processes appeared different during different observation periods and study areas, leading to differences in the composition of the elements (C, H, O, N) in the OOA. Therefore, different seasons should generate different O/C ratios.

Figs. 6(c) and 6(d) showed the average diurnal variations of the H/C, N/C, O/C and OM/OC ratios. The relative organic composition was made up of five major organic matter fragments, including $C_xH_y^+$, $C_xH_yO_z^+$, H_xO^+, $C_xH_yN_p^+$, $C_xH_yO_zN_p^+$, which decide the H/C, N/C, O/C and OM/OC ratios. The diurnal patterns of the atomic ratios were mostly attributed to diurnal changes in the relative importance of the different sources (Zhang *et al.*, 2014). Both the O/C and OM/OC ratios appeared to peak at 15:00 local time; the peak values corresponded to 0.42 and 1.70 for the O/C ratio and OM/OC ratio, respectively. The peak times occurred when the photochemical production enhanced the formation of secondary organic aerosol. It lead to the content of oxygen increasing substantially, which made the O/C ratio reach its highest value. This study found an additional, significantly lower peak at 12:00 noon. This phenomenon may have been caused by cooking activity or motor vehicle exhaust emissions, which both produce primary organic aerosols with a lower O/C ratio. These findings were similar to the results obtained by Zhang *et al.* (2014). The lowest values of the O/C and OM/OC ratios appeared at 19:00, corresponding to 0.21 and 1.37, respectively, and were related to cooking activities and evening rush hour. As expected, the H/C ratio showed a diurnal variation with a trend opposite to that of the O/C and OM/OC ratios, where the maximum (1.67) and the minimum (1.52) values occurred at 19:00 and 15:00, respectively. The N/C ratio's diurnal pattern was similar to the pattern observed for O/C and OM/OC ratios. Fig. 6(e) showed the average organic elemental compositions, with C, H, O, and N composing 72.4%, 7.3%, 16.9% and 3.4% of the total organic matter, respectively.

Back Trajectory Clustering Analysis

The Hybrid Single Particle Lagrangian Integrated Trajectory (HYSPLIT) model was used to analyze the

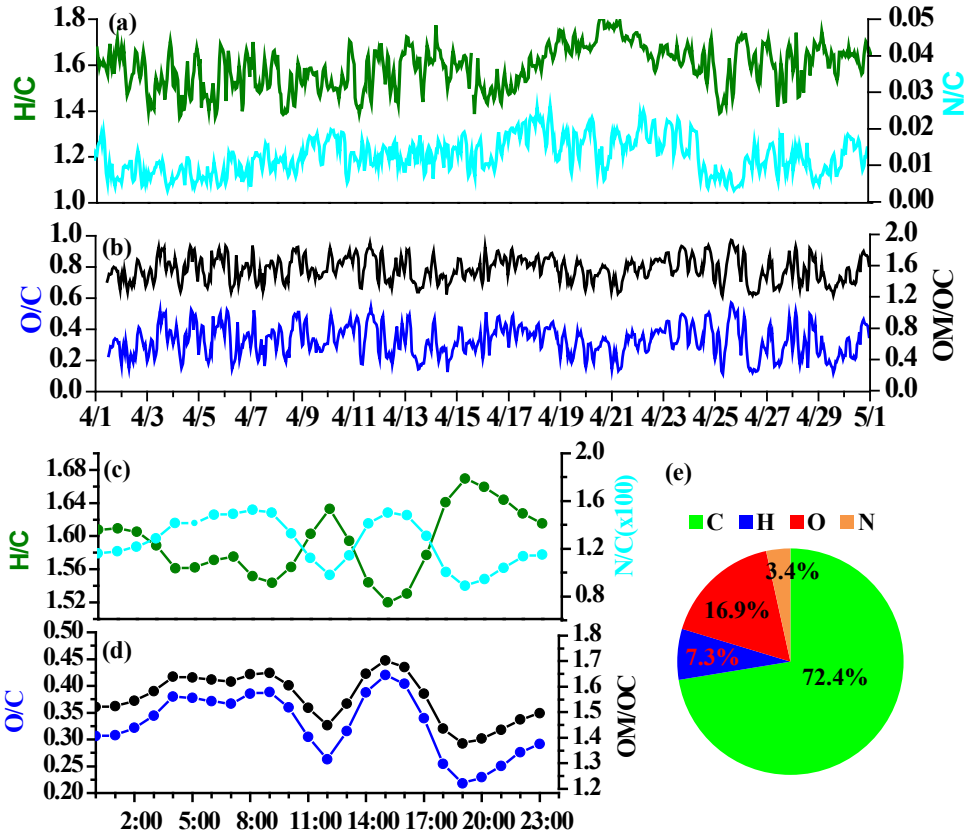

Fig. 6. The time series of (a) H/C and N/C ratios; (b) O/C and OM/OC ratios; the average diurnal variations of (c) H/C and N/C ratios and (d) O/C and OM/OC ratios; (e) the average organics elemental compositions.

influence of air current transport on NR-PM_1 loading and composition. The back trajectory analysis steps are described in detail in a previous study (HYSPLIT4 user's guide, Version 4.9, http://ready.arl.noaa.gov/HYSPLIT.php) and are briefly introduced here. First, 72 h back trajectories starting at 200 m (BT1) and 500 m (BT2) above ground level in Beijing (39.97°, 116.37°) were calculated every 6 h (at 0, 6, 12 and 18:00 local time (LT)) throughout the campaign. The back trajectories were then clustered according to their similarity in spatial distribution using the HYSPLIT4 software. As a result, the four-cluster solution was adopted according to the change in total spatial variance (Fig. 7).

BT1 and BT2 showed significant similarities. The BT1-cluster 1 (air mass frequency of 34%) and BT2-cluster 1 (air mass frequency of 33%) represented heavily polluted air mass originating from the Bohai Sea region, east of Beijing, and passed Tianjin, a large industrial city in northern China, before arriving. The corresponding NR-PM_1 mass concentrations were 87 μg m^{-3} and 82 μg m^{-3}, for BT1 and BT2, respectively. The secondary components nitrate, sulfate, ammonium and OOA dominated the NR-PM_1 composition, accounting for 25%, 23%, 19% and 10% in BT1-Cluster1 and 24%, 23%, 18% and 10% in BT2-Cluster1, respectively. Previous studies (Huang *et al.*, 2010; Zhang *et al.*, 2014) indicated that high NR-PM_1 mass concentrations were associated with southerly air pollution events.

The other three air mass clusters of BT1 and BT2 all originated from the northwest. BT1-Clusters 2 and 3 were similar and originated in the clean area of northern Beijing, but the NR-PM_1 mass concentrations showed only small differences because of the differences in the heights of the air masses. BT1-Cluster 2 was always lower than BT1-Cluster 3 before the air mass arrived in Beijing. BT1-Cluster 2 had a shorter transport distance than BT1-Cluster 3; therefore, the air mass carried more pollutants, causing the high concentrations. Long distance transport increases the dilution of the pollutants in the air mass, leading to lower concentrations. Similar results were presented in Zhang *et al.* (2014). However, there was no significant difference in NR-PM_1 mass concentrations between BT2-Cluster 2 and BT2-cluster 3, where the mass concentrations were 38 μg m^{-3} and 35 μg m^{-3}, respectively. BT1-Cluster 4 and BT2-Cluster 4 were the cleanest air mass, with corresponding mass concentrations of 22 μg m^{-3} and 23 μg m^{-3}, respectively.

CONCLUSIONS

This study systematically investigated the characteristics of submicron aerosol during spring in Beijing and the impact frequent spring dust events could have on submicron aerosol. The high temporal resolution NR-PM_1 mass concentration varied between 0.3 μg m^{-3} and 209.5 μg m^{-3}, and with an average concentration of 49.7 ± 40.2 μg m^{-3}. Organic matter was the most abundant component, accounting for 51% of the NR-PM_1, followed by sulfate (18%), nitrate (16%), ammonium (12%) and chloride (3%). The spring dust

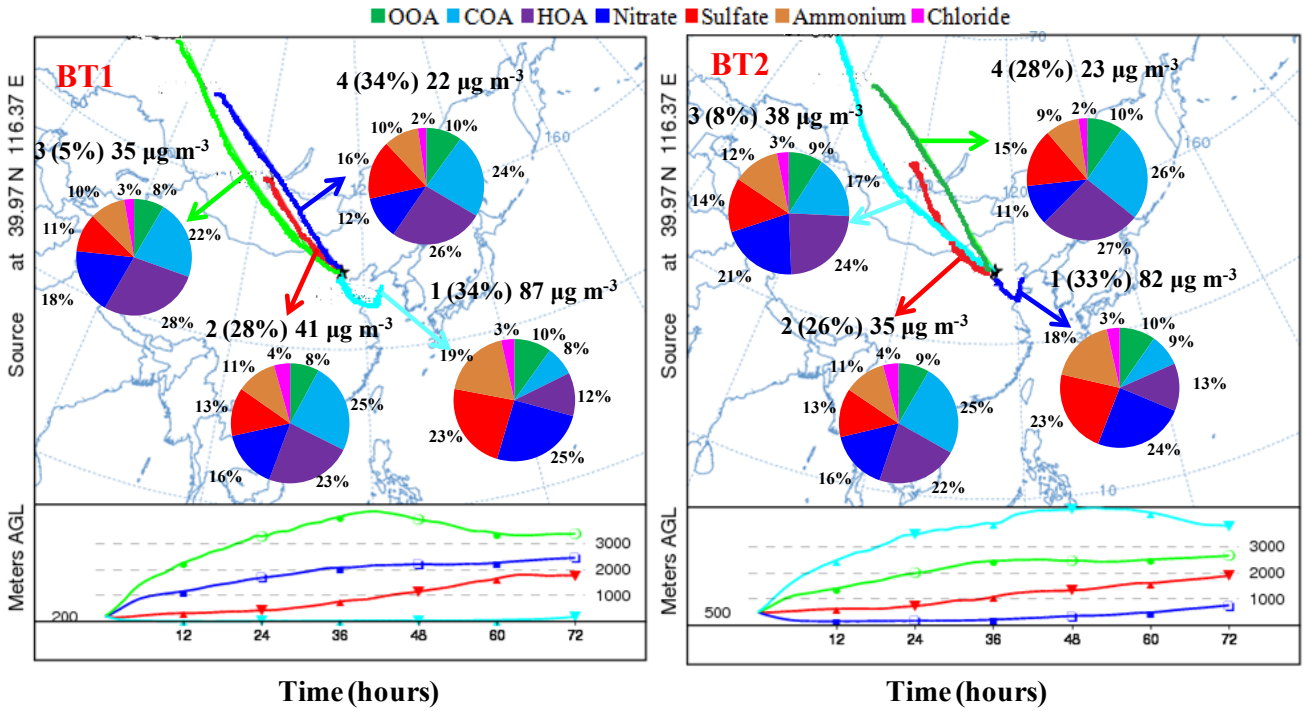

Fig. 7. Back trajectory clusters, and the corresponding mean NR-PM_1 compositions during the campaign.

originating from the northwest may have contributed more fine particles and allowed the average NR-PM_1 concentration to reach 56 μg m^{-3}. The spring dust also affected the chemical components of the fine particles, and the secondary species mass concentrations of sulfate, nitrate, ammonium and OOA increased. The measurements of the organic elemental composition indicated that the average C, H, O and N contributions to the total organic matter were 72.4%, 7.3%, 16.9% and 3.4%, respectively, and the average O/C and OM/OC ratios were 0.33 ± 0.09 and 1.55 ± 0.15, respectively. A PMF analysis performed on the high resolution organic mass spectral data found that OOA, HOA and COA accounted for 23%, 42% and 35% of organic aerosol, respectively. OOA showed a mostly stable diurnal profile, but COA and HOA showed apparent diurnal variation. COA showed peak values at noon and night, which were related to cooking activity; HOA showed higher values at night (20:00), which were related to evening motor vehicle traffic. Back trajectory clustering analysis indicated that the southeast air mass was associated with the highest NR-PM_1 loading, and was rich in oxidized organic aerosol.

ACKNOWLEDGMENTS

This study was supported by the "Strategic Priority Research Program" of the Chinese Academy of Sciences (XDB05020201). This work was also funded by Beijing Natural Science Foundation (8142034).

REFERENCES

Aiken, A.C., DeCarlo, P.F. and Jimenez, J.L. (2007). Elemental analysis of organic species with electron ionization high-resolution mass spectrometry. *Anal. Chem*. 79: 8350–8365.

Aiken, A.C., Decarlo, P.F., Kroll, J.H., Worsnop, D.R. and Huffman, J.A. (2008). O/C and OM/OC ratios of primary, secondary, and ambient organic aerosols with high-resolution time-of-flight aerosol mass spectrometry. *Environ. Sci. Technol*. 42: 4478–4485.

Aiken, A.C., Salcedo, D., Cubison, M.J., Huffman, J.A., DeCarlo, P.F., Ulbrich, I.M. and Docherty, K.S. (2009). Mexico City aerosol analysis during Milagro using high resolution aerosol mass spectrometry at the urban supersite (T0)-Part 1: Fine particle composition and organic source apportionment. *Atmos. Chem. Phys*. 9: 6633–6653.

Allan, J.D., Alfarra, M.R., Bower, K.N., Williams, P.I., Gallagher, M.W., Jimenez, J.L., McDonald, A.G., Canagaratna, M.R. and Jayne, J.T. (2003). Quantitative sampling using an Aerodyne aerosol mass spectrometer 2. Measurements of fine particulate chemical composition in two U.K. cities. *J. Geophys. Res*. 108: 4091–4105.

Arimoto, R., Kim, Y.J., Kim, Y.P., Quinn, P.K., Bates, T.S. and Anderson, T.L. (2006). Characterization of Asian dust during ACE-Asia. *Global Planet. Change* 52: 23–56.

Canagaratna, M.R., Jayne, J.T., Ghertner, A.D., Herndon, S., Shi, Q., Jimenez, J.L., Silva, P.J., Williams, P., Lanni, T. and Drewnick, F. (2004). Chase studies of particulate emissions from in-use New York City vehicles. *Aerosol Sci. Technol*. 38: 555–573.

Canagaratna, M.R., Jayne, J.T., Jimenez, J.L., Allan, J.D., Alfarra, M.R., Zhang, Q. and Onasch, T.B. (2007). Chemical and microphysical characterization of ambient aerosols with the aerodyne aerosol mass spectrometer. *Mass Spectrom. Rev*. 26: 185–222.

Chen, C., Sun, Y.L., Xu, W.Q., Du, W., Zhou, L.B., Han, T.T. and Wang, Q.Q. (2015). Characteristics and sources of submicron aerosols above the urban canopy (260 m) in Beijing, China, during the 2014 APEC summit. *Atmos. Chem. Phys*. 15: 12879–12895.

Chow, J.C., Watson, J.G., Lowenthal, D.H., Chen, L.W.A., Zielinska, B., Mazzoleni, L.R. and Magliano, K.L. (2007). Evaluation of organic markers for chemical mass balance source apportionment at the Fresno Supersite. *Atmos. Chem. Phys.* 7: 1741–1754.

DeCarlo, P.F., Kimmel, J.R., Trimborn, A., Northway, M.J., Jayne, J.T., Aiken, A.C., Gonin, M., Fuhrer, K., Horvath, T., Docherty, K.S., Worsnop, D.R. and Jimenez, J.L. (2006). Field–deployable, high-resolution, time-of-flight aerosol mass spectrometer. *Anal. Chem*. 78: 8281–8289.

DeCarlo, P.F., Ulbrich, I.M., Crounse, J., de Foy, B., Dunlea, E.J., Aiken, A.C., Knapp, D., Weinheimer, A.J., Campos, T., Wennberg, P.O. and Jimenez, J.L., (2010). Investigation of the sources and processing of organic aerosol over the Central Mexican Plateau from aircraft measurements during MILAGRO. *Atmos. Chem. Phys*. 10: 5257–5280.

Drewnick, F. , Hings, S. S., Alfarra, M. R., Prevot, A. S. H. and Borrmann, S. (2009). Aerosol quantification with the Aerodyne Aerosol Mass Spectrometer: Detection limits and ionizer background effects. *Atmos. Meas. Tech*. 2: 33–46.

Du, W., Sun, Y.L., Xu, Y. S., Jiang, Q. and Wang, Q.Q. (2015). Chemical characterization of submicron aerosol and particle growthevents at a national background site (3295ma.s.l.) on the Tibetan Plateau. *Atmos. Chem. Phys.* 15: 10811–10824.

Ge, X.L., Setyan, A., Sun, Y.L. and Zhang, Q. (2012). Primary and secondary organic aerosols in Fresno, California during wintertime: Results from high resolution aerosol mass spectrometry. *J. Geophys. Res.* 117: D19301.

Guo, S., Hu, M., Zamora, M.L., Peng, J., Shang, D., Zheng, J. and Du, Z. (2014). Elucidating severe urban haze formation in China. *Proc. Natl. Acad. Sci. U.S.A.* 111: 17373–17378.

He, L.Y., Lin, Y., Huang, X.F., Guo, S., Xue, L., Su, Q., Hu, M., Luan, S.J. and Zhang, Y. H. (2010). Characterization of high-resolution aerosol mass spectra of primary organic aerosol emissions from Chinese cooking and biomass burning. *Atmos. Chem. Phys*. 10: 11535–11543.

Hildebrandt, L., Engelhart, G.J., Mohr, C., Kostenidou, E., Lanz, V.A., Bougiatioti, A. and DeCarlo, P.F. (2010). Aged organic aerosol in the Eastern Mediterranean: The finokalia aerosol measurement experiment–2008. *Atmos. Chem. Phys*. 10: 4167–4186.

Hu, W.W., Hu, M. and Hu. W. (2016). Chemical composition, sources, and aging process of submicron aerosols in Beijing: Contrast between summer and winter. *J. Geophys. Res.* 121: 1955–1977.

Huang, X.F., He, L.Y., Hu, M., Canagaratna, M.R., Sun, Y., Zhang, Q. and Zhu, T. (2010). Highly time-resolved chemical characterization of atmospheric submicron particles during 2008 Beijing Olympic Games using an Aerodyne High-Resolution Aerosol Mass Spectrometer. *Atmos. Chem. Phys*. 10: 8933–8945.

Huang, X.F., He, L.Y., Hu, M., Canagaratna, M.R., Kroll, J.H., Ng, N.L., Zhang, Y.H., Lin, Y., Xue, L., Sun, T.L., Liu, X.G., Shao, M., Jayne, J.T. and Worsnop, D.R. (2011). Characterization of submicron aerosols at a rural site in Pearl River Delta of China using an Aerodyne High-Resolution Aerosol Mass Spectrometer. *Atmos. Chem. Phys.* 11: 1865–1877.

Huang, X.F., He, L.Y., Xue, L., Sun, T.L., Zeng, L.W., Gong, Z.H., Hu, M. and Zhu, T. (2012). Highly time-resolved chemical characterization of atmospheric fine particles during 2010 Shanghai World Expo. *Atmos. Chem. Phys*. 12: 4897–4907.

Huo, M.Q., Sun, Q. and Bai. Y.H. (2010). Chemical character of precipitation and related particles and trace gases in the North and South of China. *J. Atmos. Chem*. 69: 29–43.

Jayne, J.T., Leard, D.C., Zhang, X., Davidovits, P., Smith, K.A., Kolb, C.E. and Worsnop, R.D. (2000). Development of an aerosol mass spectrometer for size and composition analysis of submicron particles. *Aerosol Sci. Technol.* 33: 49–70.

Jimenez, J.L., Jayne, J.T., Shi, Q., Kolb, C.E., Worsnop. R.D., Yourshaw, I., Seinfeld. J.H., Flagan, R.C., Zhang, X.F., Smith, K.A. and Morris, J.W. (2003). Ambient aerosol sampling using the Aerodyne Aerosol Mass Spectrometer. *J. Geophys. Res*. 108: 8425.

Jimenez, J.L., Canagaratna, M.R., Donahue, N.M., Prevot, A.S., Zhang, Q., Kroll, J.H. and DeCarlo, P.F. (2009). Evolution of organic aerosols in the atmosphere. *Science* 326: 1525–1529.

Kubelova, L., Vodicka, P., Schwarz, J., Cusack, M., Makes, O., Ondracek, J. and Zdimal, V. (2015). A study of summer and winter highly time-resolved submicron aerosol composition measured at a suburban site in Prague. *Atmos. Environ*. 118: 45–57.

Lanz, V.A., Alfarra, M.R., Baltensperger, U., Buchmann, B. and Hueglin, C. (2007). Source apportionment of submicron organic aerosols at an urban site by factor analytical modelling of aerosol mass spectra. *Atmos. Chem. Phys.* 7: 1503–1522.

Levy, M.E., Zhang, R.Y., Zheng, J., Tan, H.B., Wang, Y., Molina, L.T., Takahama, S., Russell, L.M. and Li, G.H., (2014). Measurements of submicron aerosols at the California-Mexico border during the Cal-Mex 2010 field campaign. *Atmos. Environ*. 88: 308–319.

Liu, Z.R., Hu, B., Zhang, J.K., Yu, Y.C. and Wang. Y.S. (2016). Characteristics of aerosol size distributions and chemical compositions during wintertime pollution episodes in Beijing. *Atmos. Res*. 168: 1–12.

Middlebrook, A.M., Bahreini, R., Jimenez, J.L. and Canagaratna, M.R. (2012). Evaluation of composition-dependent collection efficiencies for the aerodyne aerosol mass spectrometer using field data. *Aerosol Sci. Technol.* 46: 258–271.

Mohr, C., Huffman, J.A., Cubison, M.J., Aiken, A.C., Docherty, K.S., Kimmel, J.R., Ulbrich, I.M., Hannigan, M. and Jimenez, J.L. (2009). Characterization of primary

organic aerosol emissions from meat cooking, trash burning, and motor vehicles with high-resolution aerosol mass spectrometry and comparison with ambient and chamber observations. *Environ. Sci. Technol*. 43: 2443–2449.

Mohr, C., DeCarlo, P.F., Heringa, M.F., Chirico, R., Slowik, J.G., Richter, R. and Reche, C. (2012). Identification and quantification of organic aerosol from cooking and other sources in Barcelona using aerosol mass spectrometer data. *Atmos. Chem. Phys*. 12: 1649–1665.

Ng, N.L., Canagaratna, M.R., Zhang, Q., Jimenez, J.L., Tian, J., Ulbrich, I.M. and Kroll, J.H. (2010). Organic aerosol components observed in Northern Hemispheric datasets from Aerosol Mass Spectrometry. *Atmos. Chem. Phys*. 10: 4625–4641.

Paatero, P. and Hopke, P.K. (2003). Discarding or downweighting high-noise variables in factor analytic models. *Anal. Chim. Acta* 490: 277–289.

Pan, Y.P., Wang, Y.S., Zhang, J.K., Liu, Z.R., Wang, L.L., Tian, S.L. and Tang, G.Q. (2016). Redefining the importance of nitrate during haze pollution to helpoptimize an emission control strategy. *Sci. Total Environ*. 141: 197–202.

Quérel, A., Lemaitre, P., Monier, M., Porcheron, E. and Flossmann, A. (2013). Study of Aerosol Particle Scavenging by Rain, Experiments and Modelling. In *Air Pollution Modeling and its Application XXII.* Steyn, D.G., Builtjes, P.J.H. and Timmermans, R.M.A. (Eds.), Springer Netherlands, Dordrecht, pp. 169–174.

Reff, A., Eberly, S.I. and Bhave, P.V. (2007). Receptor modeling of ambient particulate matter data using positive matrix factorization: Review of existing methods. *J. Air Waste Manage. Assoc*. 57: 146–154.

Seinfeld, J.H. and Pandis, S.N. (2006). *From Air Pollution to Climate Change*. Wiley, John&Sons, Incorporated, NewYork, 1203 p.

Shen, X., Lee, T., Guo, J.,Wang, X., Li, P., Xu, P. and Wang, Y. (2012). Aqueous phase sulfate production in cloudsin eastern China. *Atmos. Environ*. 62: 502–511.

Sun, J., Zhang, Q., Canagaratna, M.R., Zhang, Y., Ng, N.L., Sun, Y., Jayne, J.T., Zhang, X., Zhang, X. and Worsnop, D.R. (2010). Highly time and size-resolved characterization of submicron aerosol particles in Beijing using an Aerodyne Aerosol Mass Spectrometer. *Atmos. Environ*. 44: 131–140.

Sun, Y., Zhang, Q., Macdonald, A.M. and Hayden, K., (2009). Size-resolved aerosol chemistry on Whistler Mountain, Canada with a high–resolution aerosol mass spectrometer during INTEX–B. *Atmos. Chem. Phys*. 9: 3095–31111.

Sun, Y.L., Zhang, Q., Schwab, J.J., Chen, W.N., Bae, M.S., Lin, Y.C., Hung, H.M. and Demerjian, K.L. (2011a). A case study of aerosol processing and evolution in summer in New York City. *Atmos. Chem. Phys*. 11: 12737–12750.

Sun, Y.L., Zhang, Q., Schwab, J.J., Demerjian, K.L., Chen, W.N., Bae, M.S. and Hung, H.M. (2011b). Characterization of the sources and processes of organic and inorganic aerosols in New York City with a high-resolution time-of-flight aerosol mass apectrometer. *Atmos. Chem. Phys*. 11: 1581–1602.

Sun, Y.L., Wang, Z.F., Fu, P.Q., Jiang, Q. and Yang, T. (2013a). The impact of relative humidity on aerosol composition and evolution processes during wintertime in Beijing, China. *Atmos. Environ*. 77: 927–934.

Sun, Y.L., Wang, Z.F., Fu, P.Q., Yang, T., Jiang, Q., Dong, H.B., Li, J. and Jia, J.J. (2013b). Aerosol composition, sources and processes during wintertime in Beijing. China. *Atmos. Chem. Phys*. 13: 4577–4592.

Sun, Y.L., Wang, Z.F., Du, W., Zhang, Q., Wang, Q.Q. and Fu, P.Q. (2015). Long-term real-time measurements of aerosol particle composition in Beijing, China: seasonal variations, meteorological effects, and source analysis. *Atmos. Chem. Phys*. 15: 10149–10165.

Sun, Z., Mu, Y., Liu, Y. and Shao, L. (2013c). A comparison study on airborne particles during haze days and non-haze days in Beijing. *Sci. Total Environ*. 456–457: 1–8.

Tobo, Y., Zhang, D., Matsuki, A. and Iwasaka, Y. (2010). Asian dust particles converted into aqueous droplets under remote marine atmospheric conditions. *Proc. Natl. Acad. Sci. U.S.A*. 107: 17905–17910.

Ulbrich, I.M., Canagaratna, M.R., Zhang, Q., Worsnop, R.D. and Jimenez, J.L. (2009). Interpretation of organic components from Positive Matrix Factorization of aerosol mass spectrometric data. *Atmos. Chem. Phys*. 9: 2891–2918.

Wang, G., Li, J., Cheng, C., Hu, S., Xie, M. and Gao, S. (2011). Observation of atmospheric aerosols at Mt. Hua and Mt. Tai in central and east China during spring 2009–Part 1: EC, OC and inorganic ions. *Atmos. Chem. Phys*. 11: 4221–4235.

Wang, G.H., Li, J.J., Cheng, C.L., Zhou, B.H., Xie, M.J. and Hu, S.Y. (2012a). Observation of atmospheric aerosolsat Mt. Hua and Mt. Tai in central and east China during spring2009 – Part 2: Impact of dust storm on organic aerosol composition and size distribution. *Atmos. Chem. Phys*. 12: 4065–4080.

Wang, G.H., Zhou, B.H., Cheng, C.L., Cao, J.J., Li, J.J. and Meng, J.J. (2013). Impact of Gobi desert dust on aerosol chemistry of Xi'an, inland China during spring 2009: Differences in composition and size distribution between the urban ground surface and the mountain atmosphere. *Atmos. Chem. Phys*. 13: 819–835.

Wang, G.H., Cheng, C.L., Huang, Y., Tao, J., Ren, Y.Q. and Wu, F. (2014). Evolution of aerosol chemistry in Xian, inland China, during the dust storm period of 2013 – Part 1: Sources, chemical forms and formation mechanisms of nitrate and sulfate. *Atmos. Chem. Phys*. 14: 11571–11585.

Wang, Q.Z., Zhuang, G.S, Huang, K., Liu, T.N. and Lin, Y.F. (2016). Evolution of particulate sulfate and nitrate along the Asian dust pathway: Secondary transformation and primary pollutants via long-range transport. *Atmos. Res*. 169: 86–95.

Wang, X., Wang, W., Yang, L., Gao, X., Nie, W. and Yu, Y. (2012b). The secondary formation of inorganic aerosols in the droplet mode through heterogeneous aqueous reactions under haze conditions. *Atmos. Environ*.

63: 68–76.

Wei, Q.Y., Guo, B.B. and Cai, G.Q. (2015). The washing effect of precipitation on particulate matter and thepollution dynamics of rainwater in downtown Beijing. *Sci. Total Environ*. 505: 306–314.

Xu, W.Q., Sun, Y.L., Chen, C., Du, W., Han, T.T. and Wang, Q.Q. (2015). Aerosol composition, oxidation properties, and sources in Beijing: Results from the 2014 Asia-Pacific Economic Cooperation summit study. *Atmos. Chem. Phys*. 15: 13681–13698.

Zamora, L.M., Prospero, J.M. and Hansell, D.A. (2011). Organic nitrogen in aerosols and precipitation at Barbados and Miami: Implications regarding sources, transport and deposition to the western subtropical North Atlantic. *J. Geophys. Res.* 116: D20309.

Zhang, D.Z. and Iwasaka, Y. (1996). Nitrate and sulfate in individual Asian dust-storm particles in Beijing, China in spring of 1995 and 1996. *Atmos. Environ*. 33: 3213–3223.

Zhang, J.K., Sun, Y., Liu, Z.R., Ji, D.S., Hu, B., Liu, Q. and Wang, Y.S. (2014). Characterization of submicron aerosols during a month of serious pollution in Beijing, 2013. *Atmos. Chem. Phys*. 14: 2887–2903.

Zhang, J.K., Wang, L.L., Wang, Y.H. and Wang, Y.S. (2016). Submicron aerosols during the Beijing Asia-Pacific Economic Cooperation conference in 2014. *Atmos. Environ*. 124: 224–231.

Zhang, Q., Canagaratna, M.R. and Jayne, J.T. (2005). Time- and size-resolved chemical composition of submicron particles in Pittsburgh: Implications for aerosol sources and processes. *J. Geophys. Res*. 110: D07S09 .

Zhang, Q., Jimenez, J.L., Worsnopw, D.R. and Canagaratna, M. (2007). A case study of urban particle acidity and its influence on secondary organic aerosol. *Environ. Sci. Technol*. 41: 3213–3219.

Received for review, May 11, 2016
Revised, September 4, 2016
Accepted, October 2, 2016